

# Four-coordinate N-heterocyclic carbene (NHC) copper(I) complexes bearing functionalized 3-benzyl-1-(pyridyl)-1H-imidazolylidene ligands: Synthesis, photophysical properties and computational study

Bingbing Yang <sup>a</sup>, Jinglan Wang <sup>a</sup>, Shengxian Xu <sup>a</sup>, Hongyun Chen <sup>a</sup>, Feng Zhao <sup>a,\*</sup>, Yibo Wang <sup>b</sup>

<sup>a</sup> School of Chemistry and Chemical Engineering, Jiangxi Science and Technology Normal University, Fenglin Street Nanchang, Jiangxi 330013, PR China

<sup>b</sup> Key Laboratory of Guizhou High Performance Computational Chemistry, Department of Chemistry, Guizhou University, Guiyang 550025, PR China

## ARTICLE INFO

### Article history:

Received 22 August 2019

Accepted 6 November 2019

Available online xxxx

### Keywords:

Carbene ligand

Copper(I) complex

Photoluminescence efficiency

Excited-state lifetime

Density functional theory

## ABSTRACT

Seven luminescent copper(I) complexes bearing four-coordinate N-heterocyclic carbene (NHC) ligands with varying electron-withdrawing substituents including  $-CF_3$ ,  $-CN$ ,  $-COCH_3$ , and  $-CHO$  groups at the pyridine ring part of the carbene are reported in this study. **P1-P4** without the methyl group show better light absorption in low-energy region compared with **P5-P7** with the methyl group at the  $\alpha$ -position of the pyridine ring. The emitting state of all the complexes is regarded as the  $^3MLCT/^3LLCT$  character. **P1-P4** exhibit the emission maximum in the range of 537–547 nm with the photoluminescence quantum yields (PLQY) of 12.7–21.9% in PMMA films and excited state lifetimes ( $\tau$ ) of 14.7–22.6  $\mu$ s. The emission wavelengths of **P5-P7** are blue-shifted to 505–513 nm compared with those of **P1-P4**, showing the higher PLQY of 38.0–57.3% and longer  $\tau$  of 36.2–84.8  $\mu$ s. Theoretical calculations were used to rationalize the photophysical properties.

© 2019 Elsevier Ltd. All rights reserved.

## 1. Introduction

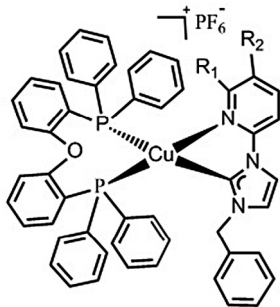
Copper(I) complexes have important application as the emitting component layer in lighting field because of their lower cost and toxicities [1–5]. However, their low photoluminescence efficiency makes them less popular compared with other noble metal complexes in OLED fields because of their flexible geometry framework and smaller spin-orbit coupling [6,7]. The structure distortion of the complexes, which seriously increase the nonradiative decay, must be suppressed to improve the photoluminescence efficiency. Many advances have been achieved in designing strongly luminescent Cu(I) complexes in recent years [8–12]. A particularly important class of these complexes is the  $[Cu(N^N)(P^P)]^+$  complexes with the mixed-ligand, where  $N^N$  is a diimine ligand (including 2,2'-bipyridine, 1,10-phenanthroline, or their derivatives) and the ancillary ligand,  $P^P$ , denotes diphosphine ligands (such as bis[2-(diphenylphosphino)phenyl]ether (POP)) [13–17]. Although these complexes are known to exhibit remarkable photophysical properties, it is still highly desirable to develop a novel family of luminescence Cu(I) complexes by the structure modification of the ligands.

Very recently, many research groups [18–22] have been interested in employing N-heterocyclic carbene (NHC) ligand to prepare

emissive NHC-Cu(I) complexes because it possesses strong  $\sigma$  donation ability and the stability of the corresponding complex [23]. So far, most of these complexes reported have a three-coordinate geometry around the Cu center with the formula  $[Cu(NHC)(N^N)]^{0/+1}$ , where the NHC ligand acts as a monodentate ligand, while the  $N^N$  ligand is a chelating diimine. Many of these complexes show the high photoluminescence quantum efficiencies and long excited state lifetimes. However, nearly all of the reported complexes were synthesized using a very bulky monodentate ligand, 1,3-bis(2,6-diisopropylphenyl)imidazol-2-ylidene (IPr). Thus, selection scope of the demanding NHC ligand is rather limited. On the other hand, NHC-Cu(I) complexes with the four-coordinate geometry should be a potent choice in this hot topic. To our surprise, studies on the synthesis and emission properties related to the four-coordinate NHC-Cu(I) complexes are relatively rare. Recently, our group and Wang et al. [24–28] synthesized this type of complexes. NHC-Cu(I) complexes can be easily prepared from the commercially available Cu powders as the starting materials [24]. These types of complexes all exhibit high emissive quantum yields due to the high rigidity of the framework. Through this route, we reported the synthesis of a series of the similar structural complexes, and the corresponding photophysical properties can be tailored by varying different aryl substituents bound to the NHC ligands [25,26]. Notably, our results showed that the NHC-Cu(I) complexes containing the benzyl-substituted imidazolylidene ring

\* Corresponding author.

E-mail address: zhf19752003@163.com (F. Zhao).



<b>P1</b> ( $R_1 = H, R_2 = CF_3$ )
<b>P2</b> ( $R_1 = H, R_2 = CN$ )
<b>P3</b> ( $R_1 = H, R_2 = COCH_3$ )
<b>P4</b> ( $R_1 = H, R_2 = CHO$ )
<b>P5</b> ( $R_1 = CH_3, R_2 = CN$ )
<b>P6</b> ( $R_1 = CH_3, R_2 = Br$ )
<b>P7</b> ( $R_1 = CH_3, R_2 = F$ )

Fig. 1. Chemical structure of the NHC-Cu(I) complexes **P1–P7**.

have higher photoluminescence efficiencies than the analogous ones containing naphthyl and anthryl substituents.

With the aim of expanding our work and motivated by the rich photophysical properties of the type of complexes, we present the preparation of a series of the NHC-Cu(I) complexes containing different electron-withdrawing groups attached at the  $\alpha$ -position of pyridine ring, remaining the benzyl-substituted imidazolylidene ring unchanged (Fig. 1). The excellent photophysical properties of these complexes make them suitable for future application as OLED emitters. The photophysical properties were comprehensively investigated using experimental and theoretical methods.

## 2. Experimental

### 2.1. Materials and methods

Chemical reagents were obtained from Sinopharm Chemical Reagent Co Ltd. and used without further purification. A Bruker AV400 MHz spectrometer was utilized to obtain the  $^1\text{H}$  NMR spectra. An Agilent 6450 Q-TOF mass spectrometer was used to obtain high-resolution mass spectra (HRMS). An Elementar VarioEL cube analyzer was employed to obtain elemental analysis data (C, H, and N) of the complexes. Crystallographic data of **P7** were analyzed on a Bruker SMART APEX II CCD diffractometer using a multiscan-technique. The structure has been deposited as supplemental material at the Cambridge Crystallographic Data Center CCDC 1906684. A Perkin Elmer Lambda-900 spectrophotometer and a Hitachi F-4600 spectrophotometer were used to record UV-Vis absorption and emission spectra, respectively. A Hamamatsu-C11347 system equipped with an integrating sphere was employed to obtain absolute photoluminescence quantum yields. The excited state lifetimes were measured using a Hamamatsu C11367 spectrometer.

### 2.2. Synthetic procedure

Compounds **1–7**, ligands **L1–L7** and the corresponding complexes **P1–P7** were synthesized according to the similar method in our previously paper [24]. The structural data were listed in the following:

**2-(1*H*-imidazol-1-yl)-5-(trifluoromethyl) pyridine (**1**).** White solid. Yield: 0.78 g, 46%.  $^1\text{H}$  NMR (400 MHz, DMSO)  $\delta$  8.87 (s, 1H), 8.65 (s, 1H), 8.42 (d,  $J = 8.6$  Hz, 1H), 8.05 (d,  $J = 9.9$  Hz, 2H), 7.17 (s, 1H).

**6-(1*H*-imidazol-1-yl)nicotinonitrile (**2**).** Pale white solid. Yield: 0.89 g, 66%.  $^1\text{H}$  NMR (400 MHz, DMSO)  $\delta$  8.98 (s, 1H), 8.65 (s, 1H), 8.54 (d,  $J = 8.6$  Hz, 1H), 8.05 (d,  $J = 7.9$  Hz, 2H), 7.18 (s, 1H).

**6-(1*H*-imidazol-1-yl)nicotinaldehyde (**3**).** White solid. Yield: 0.68 g, 49%.  $^1\text{H}$  NMR (400 MHz, DMSO)  $\delta$  10.08 (s, 1H), 9.00 (s, 1H), 8.67 (s, 1H), 8.42 (d,  $J = 8.5$  Hz, 1H), 8.18–7.90 (m, 2H), 7.18 (s, 1H).

**1-(6-(1*H*-imidazol-1-yl)pyridin-3-yl)ethanone (**4**).** Yellow solid. Yield: 0.59 g, 40%.  $^1\text{H}$  NMR (400 MHz, DMSO)  $\delta$  9.03 (s, 1H), 8.65 (s, 1H), 8.46 (d,  $J = 8.6$  Hz, 1H), 8.05 (s, 1H), 7.96 (d,  $J = 8.6$  Hz, 1H), 7.17 (s, 1H), 2.64 (s, 3H).

**3-fluoro-6-(1*H*-imidazol-1-yl)-2-methylpyridine (**5**).** White solid. Yield: 0.72 g, 51%.  $^1\text{H}$  NMR (400 MHz, DMSO)  $\delta$  8.62 (d,  $J = 69.9$  Hz, 1H), 8.14–7.86 (m, 2H), 7.85–7.72 (m, 1H), 7.38–7.09 (m, 1H), 2.72–2.44 (m, 3H).

**3-bromo-6-(1*H*-imidazol-1-yl)-2-methylpyridine (**6**).** This compound was prepared via a similar procedure for **1** from 2,5-Dibromo-6-methylpyridine (1.99 g, 8 mmol). Yield: 1.02 g, 54%.  $^1\text{H}$  NMR (400 MHz, DMSO)  $\delta$  8.52 (s, 1H), 8.19 (d,  $J = 8.4$  Hz, 1H), 7.93 (s, 1H), 7.61 (d,  $J = 8.5$  Hz, 1H), 7.12 (s, 1H), 2.59 (s, 3H).

**6-(1*H*-imidazol-1-yl)-2-methylnicotinonitrile (**7**).** Yield: 0.79 g, 52%.  $^1\text{H}$  NMR (400 MHz, DMSO)  $\delta$  8.63 (s, 1H), 8.45 (d,  $J = 8.2$  Hz, 1H), 8.02 (s, 1H), 7.86 (d,  $J = 8.4$  Hz, 1H), 7.17 (s, 1H), 2.70 (s, 3H).

**(Ph-Im-triflumePy)(PF<sub>6</sub>) (**L1**).** Yield: 0.34 g, 30%. m.p. 122 °C.  $^1\text{H}$  NMR (400 MHz, DMSO)  $\delta$  10.38 (s, 1H), 9.11 (s, 1H), 8.84–8.52 (m, 2H), 8.27 (d,  $J = 8.6$  Hz, 1H), 8.08 (s, 1H), 7.76–7.27 (m, 5H), 5.66 (d,  $J = 73.6$  Hz, 2H).

**(Ph-Im-cyPy)(PF<sub>6</sub>) (**L2**).** Yield: 0.86 g, 85%. m.p. 210 °C.  $^1\text{H}$  NMR (400 MHz, DMSO)  $\delta$  10.38 (s, 1H), 9.18 (s, 1H), 8.77 (d,  $J = 8.5$  Hz, 1H), 8.61 (s, 1H), 8.24 (d,  $J = 8.6$  Hz, 1H), 8.08 (s, 1H), 7.47 (dt,  $J = 23.3, 8.0$  Hz, 5H), 5.55 (s, 2H).

**(Ph-Im-alPy)(PF<sub>6</sub>) (**L3**).** Yield: 0.74 g, 72%. m.p. 203 °C.  $^1\text{H}$  NMR (400 MHz, DMSO)  $\delta$  10.40 (s, 1H), 10.18 (s, 1H), 9.16 (s, 1H), 8.65 (d,  $J = 8.6$  Hz, 2H), 8.22 (d,  $J = 8.5$  Hz, 1H), 8.08 (s, 1H), 7.47 (dt,  $J = 16.4, 8.0$  Hz, 5H), 5.55 (s, 2H).

**(Ph-Im-AcPy)(PF<sub>6</sub>) (**L4**).** Yield: 0.67 g, 63%. m.p. 144 °C.  $^1\text{H}$  NMR (400 MHz, DMSO)  $\delta$  10.37 (s, 1H), 9.15 (s, 1H), 8.78–8.53 (m, 2H), 8.24–7.95 (m, 2H), 7.66–7.28 (m, 5H), 5.55 (s, 2H), 2.70 (s, 3H).

**(Ph-Im-flumePy)(PF<sub>6</sub>) (**L5**).** Yield: 0.69 g, 67%. m.p. 229 °C.  $^1\text{H}$  NMR (400 MHz, DMSO)  $\delta$  10.17 (s, 1H), 8.48 (s, 1H), 8.09 (t,  $J = 8.7$  Hz, 1H), 8.02 (s, 1H), 7.93 (d,  $J = 8.6$  Hz, 1H), 7.52 (s, 1H), 7.51 (s, 1H), 7.45 (d,  $J = 6.3$  Hz, 1H), 7.41 (d,  $J = 8.7$  Hz, 1H), 5.53 (s, 2H), 4.39 (t,  $J = 4.8$  Hz, 2H), 2.53 (d,  $J = 8.8$  Hz, 3H).

**(Ph-Im-bromePy)(PF<sub>6</sub>) (**L6**).** Yield: 0.64 g, 54%. m.p. 179 °C.  $^1\text{H}$  NMR (400 MHz, DMSO)  $\delta$  10.22 (s, 1H), 8.52 (s, 1H), 8.45 (d,  $J = 8.6$  Hz, 1H), 8.03 (s, 1H), 7.82 (d,  $J = 8.6$  Hz, 1H), 7.51 (d,  $J = 6.3$  Hz, 2H), 7.43 (d,  $J = 7.5$  Hz, 3H), 5.53 (s, 2H), 2.67 (s, 3H).

**(Ph-Im-cymePy)(PF<sub>6</sub>) (**L7**).** Yield: 0.39 g, 37%. m.p. 114 °C.  $^1\text{H}$  NMR (400 MHz, DMSO)  $\delta$  10.32 (s, 1H), 8.69 (d,  $J = 8.5$  Hz, 1H), 8.59 (s, 1H), 8.06 (d,  $J = 8.2$  Hz, 2H), 7.52 (d,  $J = 7.2$  Hz, 2H), 7.48–7.36 (m, 3H), 5.55 (s, 2H), 2.78 (s, 3H).

**P1.** Yellow powder. Yield: 0.2 g, 48%. m.p. 306 °C.  $^1\text{H}$  NMR (400 MHz, DMSO)  $\delta$  8.51 (d,  $J = 10.9$  Hz, 2H), 8.31 (d,  $J = 8.7$  Hz, 1H), 7.91 (s, 1H), 7.52 (s, 1H), 7.47–7.28 (m, 11H), 7.26–7.13 (m, 10H), 7.02 (dt,  $J = 26.6, 7.4$  Hz, 4H), 6.90–6.70 (m, 6H), 6.53 (s, 2H), 5.27 (s, 2H). Anal. Calcd. For  $C_{52}\text{H}_{40}\text{CuF}_9\text{N}_3\text{OP}_3$  (1050.35): C 59.46, H 3.84, N 4.00; found: C 59.62, H 3.58, N 4.33. HRMS ( $m/z$ , ESI $^+$ ): calcd. For  $C_{52}\text{H}_{40}\text{CuF}_3\text{N}_3\text{OP}_2$  ([M] $^+$ ) 904.1895; found 904.1847.

**P2.** Yellow powder. Yield: 0.21 g, 51%. m.p. 307 °C.  $^1\text{H}$  NMR (400 MHz, DMSO)  $\delta$  10.38 (s, 1H), 9.18 (s, 1H), 8.77 (d,  $J = 8.5$  Hz, 1H), 8.65–8.45 (m, 2H), 8.41–8.14 (m, 2H), 8.06 (d,  $J = 15.0$  Hz, 2H), 7.53 (d,  $J = 7.5$  Hz, 3H), 7.49–6.96 (m, 21H), 6.89 (s, 3H), 6.77 (d,  $J = 7.4$  Hz, 1H), 6.59 (s, 1H), 5.55 (s, 2H). Anal. Calcd. For  $C_{52}\text{H}_{40}\text{CuF}_6\text{N}_4\text{OP}_3$  (1007.36): C 62.00, H 4.00, N 5.56; found: C 61.62, H 3.88, N 5.72. HRMS ( $m/z$ , ESI $^+$ ): calcd. For  $C_{52}\text{H}_{40}\text{CuF}_3\text{N}_3\text{OP}_2$  ([M] $^+$ ) 861.1973; found 861.1969.

**P3.** Yellow powder. Yield: 0.18 g, 45%. m.p. 311 °C.  $^1\text{H}$  NMR (400 MHz, DMSO)  $\delta$  9.71 (s, 1H), 8.48 (d,  $J = 12.7$  Hz, 2H), 8.26 (d,  $J = 8.5$  Hz, 2H), 7.55 (s, 1H), 7.32 (ddt,  $J = 26.9, 14.0, 7.6$  Hz, 17H), 7.18–6.95 (m, 10H), 6.86–6.76 (m, 5H), 6.59 (s, 2H), 5.14 (s, 2H). Anal. Calcd. For  $C_{53}\text{H}_{43}\text{CuF}_6\text{N}_3\text{O}_2\text{P}_3$  (1024.39): C 62.14, H 4.23, N 5.56; found: C 61.62, H 3.88, N 5.72. HRMS ( $m/z$ , ESI $^+$ ): calcd. For  $C_{52}\text{H}_{40}\text{CuN}_4\text{OP}_2$  ([M] $^+$ ) 861.1973; found 861.1969.

4.10; found: C 62.03, H 4.12, N 4.02. HRMS (*m/z*, ESI<sup>+</sup>): calcd. For C<sub>53</sub>H<sub>43</sub>CuN<sub>3</sub>O<sub>2</sub>P<sub>2</sub> ([M]<sup>+</sup>) 878.2127; found 878.2133.

**P4.** Yellow powder. Yield: 0.176 g, 43%. m.p. 297 °C. <sup>1</sup>H NMR (400 MHz, DMSO) δ 8.56–8.42 (m, 2H), 8.21 (d, *J* = 8.5 Hz, 2H), 7.52 (s, 1H), 7.47–7.11 (m, 21H), 7.03 (dt, *J* = 26.4, 7.4 Hz, 4H), 6.91–6.64 (m, 6H), 6.55 (s, 2H), 5.26 (s, 2H), 2.22 (s, 3H). Anal. Calcd. For C<sub>52</sub>H<sub>41</sub>CuF<sub>6</sub>N<sub>3</sub>O<sub>2</sub>P<sub>3</sub> (1010.36): C 61.82, H 4.09, N 4.16; found: C 62.04, H 4.15, N 4.02. HRMS (*m/z*, ESI<sup>+</sup>): calcd. For C<sub>52</sub>H<sub>41</sub>CuN<sub>3</sub>O<sub>2</sub>P<sub>2</sub> ([M]<sup>+</sup>) 864.1970; found 864.1975.

**P5.** White powder. Yield: 0.23 g, 57%. m.p. 291 °C. <sup>1</sup>H NMR (400 MHz, DMSO) δ 8.36 (s, 1H), 8.10 (t, *J* = 8.1 Hz, 1H), 8.00 (d, *J* = 7.1 Hz, 1H), 7.47–7.36 (m, 8H), 7.28 (t, *J* = 6.5 Hz, 8H), 7.22–7.04 (m, 11H), 6.91 (s, 4H), 6.78 (s, 2H), 6.70 (d, *J* = 7.2 Hz, 2H), 5.24 (d, *J* = 28.0 Hz, 2H), 1.72 (s, 3H). Anal. Calcd. For C<sub>53</sub>H<sub>42</sub>CuF<sub>6</sub>N<sub>4</sub>OP<sub>3</sub> (1021.38): C 62.32, H 4.14, N 5.49; found: C 62.14, H 4.08, N 5.36. HRMS (*m/z*, ESI<sup>+</sup>): calcd. For C<sub>53</sub>H<sub>42</sub>CuN<sub>4</sub>OP<sub>2</sub> ([M]<sup>+</sup>) 875.2130; found 875.2145.

**P6.** White powder. Yield: 0.21 g, 52%. m.p. 271 °C. <sup>1</sup>H NMR (400 MHz, DMSO) δ 8.36 (d, *J* = 8.7 Hz, 2H), 7.87 (d, *J* = 8.6 Hz, 1H), 7.38 (dd, *J* = 22.7, 15.1 Hz, 8H), 7.26 (t, *J* = 7.3 Hz, 7H), 7.20–6.99 (m, 11H), 6.87 (s, 4H), 6.75 (s, 2H), 6.68 (d, *J* = 7.9 Hz, 2H), 5.21 (s, 2H), 1.83 (s, 3H). Anal. Calcd. For C<sub>52</sub>H<sub>42</sub>BrCuF<sub>6</sub>N<sub>3</sub>OP<sub>3</sub> (1075.27): C 58.08, H 3.94, N 3.91; found: C 58.14, H 4.02, N 3.36. HRMS (*m/z*, ESI<sup>+</sup>): calcd. For C<sub>52</sub>H<sub>42</sub>BrCuN<sub>3</sub>OP<sub>2</sub> ([M]<sup>+</sup>) 928.1282; found 928.1277.

**P7.** Yellow powder. Yield: 0.27 g, 67%. m.p. 263 °C. <sup>1</sup>H NMR (400 MHz, DMSO) δ 8.60 (d, *J* = 8.5 Hz, 1H), 8.42 (s, 1H), 8.09 (d, *J* = 8.6 Hz, 1H), 7.48 (s, 1H), 7.38 (dd, *J* = 14.8, 7.3 Hz, 6H), 7.26 (s, 8H), 7.22–7.00 (m, 11H), 6.89 (s, 4H), 6.78–6.65 (m, 4H), 5.25 (s, 2H), 1.89 (s, 3H). Anal. Calcd. For C<sub>52</sub>H<sub>42</sub>CuF<sub>7</sub>N<sub>3</sub>OP<sub>3</sub> (1014.37): C 61.57, H 4.17, N 4.14; found: C 61.35, H 4.07, N 4.08. HRMS (*m/z*, ESI<sup>+</sup>): calcd. For C<sub>52</sub>H<sub>42</sub>CuFN<sub>3</sub>OP<sub>2</sub> ([M]<sup>+</sup>) 868.2083; found 868.2088.

### 2.3. DFT calculations

The singlet geometries (S<sub>0</sub> state) of all complexes were optimized using the B3LYP functional [29,30] associated with the PCM [31] model in CH<sub>2</sub>Cl<sub>2</sub> media under Gaussian 09 [32]. The 6-31G\* basis set [33,34] was used for the C, H, N, O, and P atoms, whereas the LANL2DZ basis set [35] was employed for the Cu atom. The simulated UV-Vis spectra were calculated using the TDDFT method [36,37] in CH<sub>2</sub>Cl<sub>2</sub> media on the basis of the optimized S<sub>0</sub>

geometries. Multiwfn [38] and VMD software [39] were used for visualizing the frontier molecular orbitals.

## 3. Results and discussion

### 3.1. Synthesis and characterization

The pyridyl-imidazole derivatives **1–7** can be prepared through the C–N coupling reaction [40]. The pyridyl-imidazolium salts **L1–L7** were synthesized as previously described (Scheme 1) [41]. **P1–P7** were synthesized by the reported synthetic method [24]. The corresponding analysis data, including <sup>1</sup>H NMR, HRMS and elemental analyses, support the structures of these complexes (see Experimental Section).

complex **P7** (CCDC 1906684) was crystallized from CH<sub>2</sub>Cl<sub>2</sub>/CH<sub>3</sub>-CH<sub>2</sub>OH solution of complexes with slow evaporation speed. The crystal structure is shown in Fig. 2. The X-ray analysis reveals that

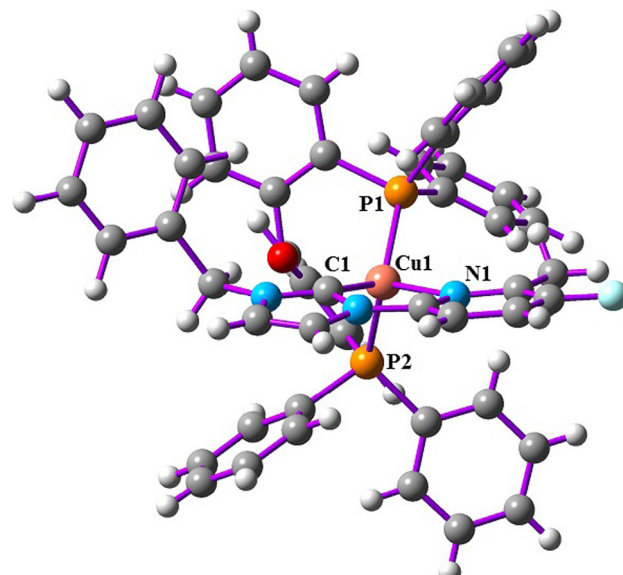
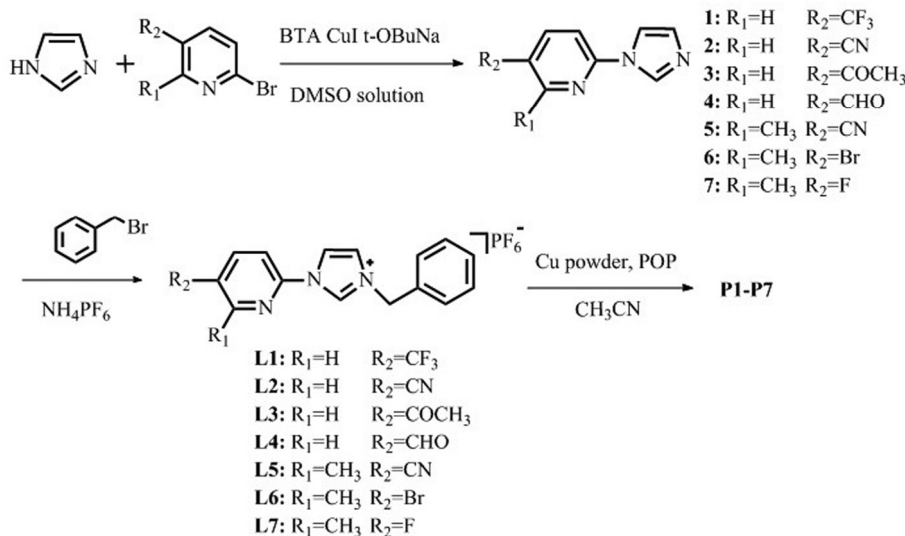


Fig. 2. X-ray crystal structure of **P7** (50% probability thermal ellipsoids).



Scheme 1. Synthetic route for complexes **P1–P7**.

two phosphorus atoms (P1, P2) of the POP ligand and one nitrogen atom (N1) of the pyridine moiety bind to the metal Cu ion center, while the fourth coordination site is occupied by a carbene carbon atom (C1) of imidazolylidene ring, thus leading to a four-coordinated tetrahedral geometry. The Cu...O separation of 3.001 Å is shorter than 3.20 Å, indicating minimum interaction between O atom and Cu(I) center. The dihedral angle between the N1-Cu1-C1 and P1-Cu1-P2 planes is a measurement of the degree of the flattening distortion of the Cu(I) complexes, which is 90° for the idealized tetrahedral geometry. Here, this angle in complex **7** is 80.5°, indicating the presence of a significant flattening distortion. This flattening distortion is caused by intramolecular steric interaction between the methyl groups at  $\alpha$ -position of the pyridine moiety and phenyl ring of POP ligand, which severely influences the photophysical properties of the complexes (see below). The lengths of Cu–P bond range from 2.259 to 2.295 Å and these data are similar to those of the Cu(I) complexes reported. The length of the Cu–C<sub>carbene</sub> bond is 1.976 Å, which is much shorter than that of the Cu–N1 distance (2.333 Å) due to the stronger bond between the carbene carbon and Cu atoms.

### 3.2. Photophysical properties

The UV–Vis spectra of **P1–P7** in CH<sub>2</sub>Cl<sub>2</sub> are provided in Fig. 3 and the important photophysical parameters are collected in Table 1. Intense bands ( $\varepsilon > 2.19 \times 10^4 \text{ M}^{-1} \text{ cm}^{-1}$ ) in the 250–300 nm region

for all these complexes correspond to carbene- and POP-based  $\pi \rightarrow \pi^*$  intraligand transitions. For the series **P1–P4**, the weaker shoulder in 350–450 nm ( $\varepsilon < 1.64 \times 10^4 \text{ M}^{-1} \text{ cm}^{-1}$ ) can be confidently regarded as metal Cu to ligand charge transfer (<sup>1</sup>MLCT). The onset of this <sup>1</sup>MLCT absorption band slightly shifts to lower energy from **P1** to **P4**, which is consistent with the energy gap energy in the order **P4** < **P3** < **P2** < **P1**. Support for this notion is seen in the theoretical results discussed below. Unlike **P1–P4**, **P5–P7** exhibit very weak <sup>1</sup>MLCT bands between 300 and 400 nm ( $\varepsilon < 0.78 \times 10^4 \text{ M}^{-1} \text{ cm}^{-1}$ ). This significant decrease in absorption ability is confidently attributed to the presence of the methyl group at the  $\alpha$ -position of the pyridine ring for **P5–P7**. This condition causes the steric hindrance with the POP ligand, thereby leaving the pyridine ring away from the Cu atom. Thus, the probability of  $S_0 \rightarrow S_1$  transition (<sup>1</sup>MLCT band) from Cu to the pyridine ring decreases and consequently exhibits the weak absorption feature.

The emission spectra of **P1–P7** in the solid state are provided in Fig. 4. The broad and unstructured emissions can be observed for all of the complexes in the green spectral region from 505 to 547 nm, which can be assigned as the triplet <sup>3</sup>MLCT character. As shown in Fig. 4, the blue-shift of the emission maximum for **P5–P7** can be observed compared with that of **P1–P4**. In addition, **P5–P7** also show much higher photoluminescence quantum yields (PLQY) (38%–57.3%) than **P1–P4** (12.7%–21.9%, Table 1). The presence of the methyl substituent at the  $\alpha$ -position of pyridine plays a crucial role for the enhancement of the PLQY as it restricts

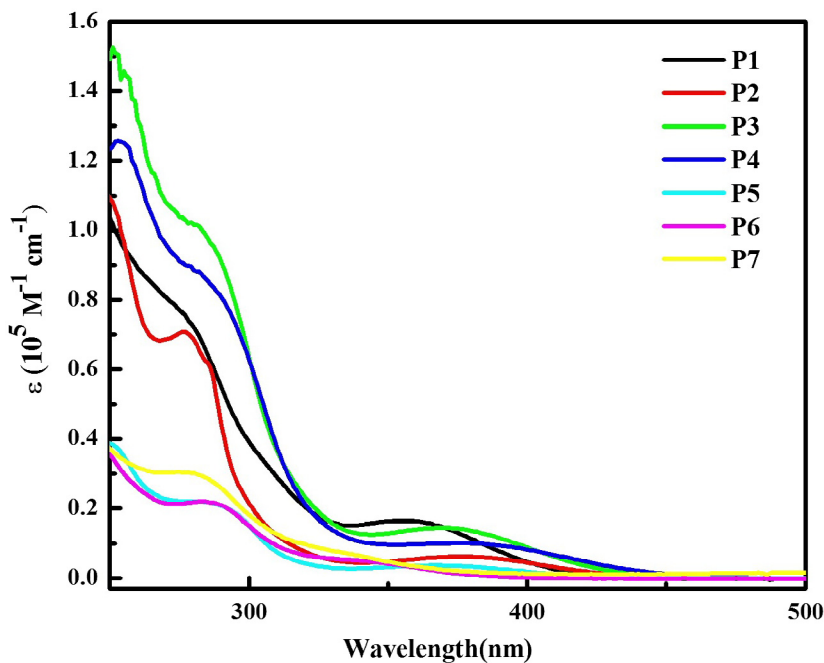


**Fig. 3.** Absorption spectra in dichloromethane at 298 K of complexes **P1–P7**.

**Table 1**  
Photophysical properties of complexes **P1–P7**.

	Absorption		Emission			
	$\lambda_{\text{abs}}/\text{nm}$ ( $\varepsilon \times 10^4 \text{ M}^{-1} \text{ cm}^{-1}$ )	$\lambda_{\text{em}}/\text{nm}$	$\tau/\mu\text{s}$	PLQY/%	$k_t/10^4 \text{ s}^{-1}$	$k_{\text{nr}}/10^4 \text{ s}^{-1}$
<b>P1</b>	272 (7.93), 355 (1.64)	537	22.6	17.3	0.77	3.66
<b>P2</b>	276 (7.10), 376 (0.63)	547	21.5	16.9	0.79	3.87
<b>P3</b>	282 (10.1), 369 (1.45)	547	18.5	21.9	1.18	4.22
<b>P4</b>	282 (8.74), 376 (1.01)	547	14.7	12.7	0.86	5.94
<b>P5</b>	274 (2.20), 367 (0.38)	531	36.2	52.3	1.44	1.32
<b>P6</b>	282 (2.19), 334 (0.53)	515	84.8	57.3	0.68	0.50
<b>P7</b>	272 (3.04), 331 (0.78)	505	40.7	38.0	0.93	1.52

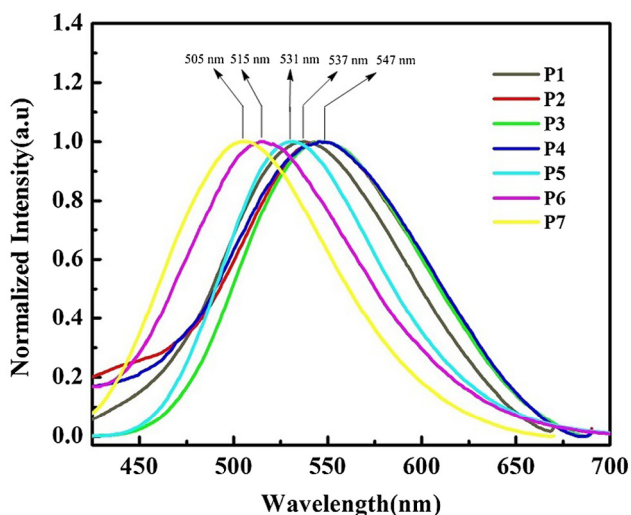


**Fig. 4.** Normalized emission spectra of **P1-P7** in PMMA films (10 wt%).

structural relaxation in the excited state, which is corroborated by the results obtained from DFT calculations (see below). The complexes showing the higher PLQY also have longer excited state lifetimes ( $\tau = 36.2\text{--}84.8 \mu\text{s}$  for **P5-P7**) compared with other complexes ( $\tau = 14.7\text{--}22.6 \mu\text{s}$  for **P1-P4**). On the basis of the known values of PLQY and  $\tau$ , the radiative rate ( $k_r$ ) and the nonradiative rate constants ( $k_{nr}$ ) can be obtained (Table 1). Although the  $k_r$  values of **P1-P4** ( $k_r = (0.77\text{--}1.18) \times 10^4 \text{ s}^{-1}$ ) are comparable to those of **P5-P7** ( $k_r = (0.68\text{--}1.44) \times 10^4 \text{ s}^{-1}$ ), the  $k_{nr}$  values of **P1-P4** ( $k_{nr} = (3.66\text{--}5.94) \times 10^4 \text{ s}^{-1}$ ) are greater than those of **P5-P7** ( $k_{nr} = (0.50\text{--}1.52) \times 10^4 \text{ s}^{-1}$ ). Thus, it is concluded that the dramatically improved photophysical properties of the series **P5-P7** is mainly due to the additional methyl groups at the  $\alpha$ -position of pyridine ring by the effective suppression of the non-radiative decay process. Additionally, the electron-donating nature of the methyl substituent also has important influences for the improvement of the photophysical properties of the complexes given that the incorporation of the methyl substituent at the  $\alpha$ -position of pyridine ring upshifts the  $\pi^*$  orbital energies of the complexes and therefore results in the blue-shift of the emission wavelength.

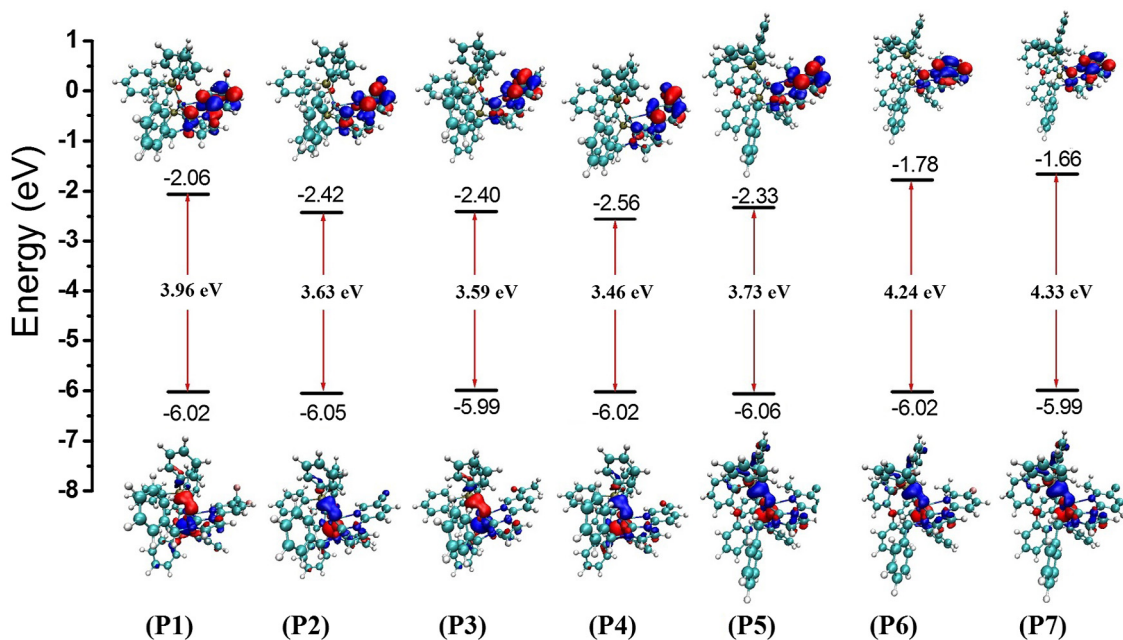


**Fig. 5.** Energies and electron density distributions for the HOMO and LUMO of **P1-P7**.

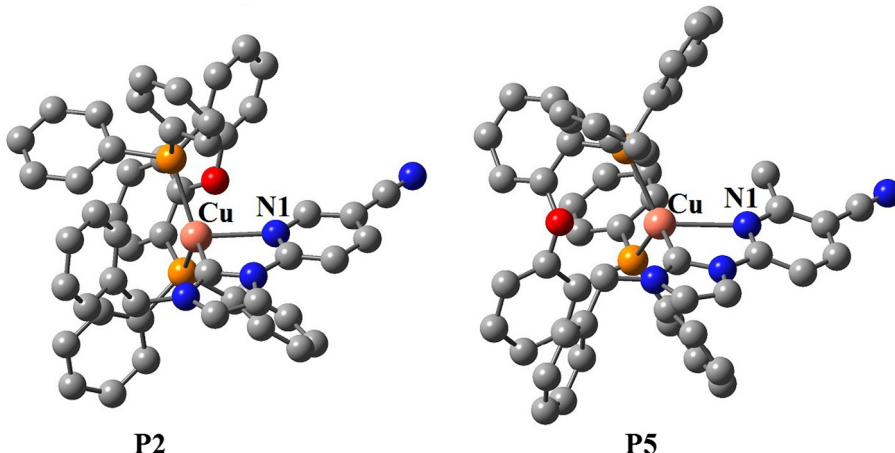


**Fig. 6.** Molecular structures of **P2** and **P5** in the  $S_0$  states.

### 3.3. Theoretical calculations

The molecular geometries of all complexes were optimized, and the structural parameters of the representative complex **P7** are in good agreement with X-ray crystal data (**Fig. 1S** and **Table 1S**, **Supporting Information**); this ensures a proper description of the electronic structures for all complexes. To extensively explore the

relationship between the properties and structure of the investigated complexes, the highest occupied molecular orbital (HOMO) and lowest unoccupied molecular orbital (LUMO) of complexes were theoretically calculated at B3LYP/6-31G(d)/LANL2DZ levels in  $\text{CH}_2\text{Cl}_2$  solution (**Fig. 5**). As shown in the figure, the HOMO is centered on the metal Cu atom and POP ligand for **P1-P7**. The HOMO energies of **P1-P7** are similar ( $-5.99$  eV to  $-6.06$  eV). On

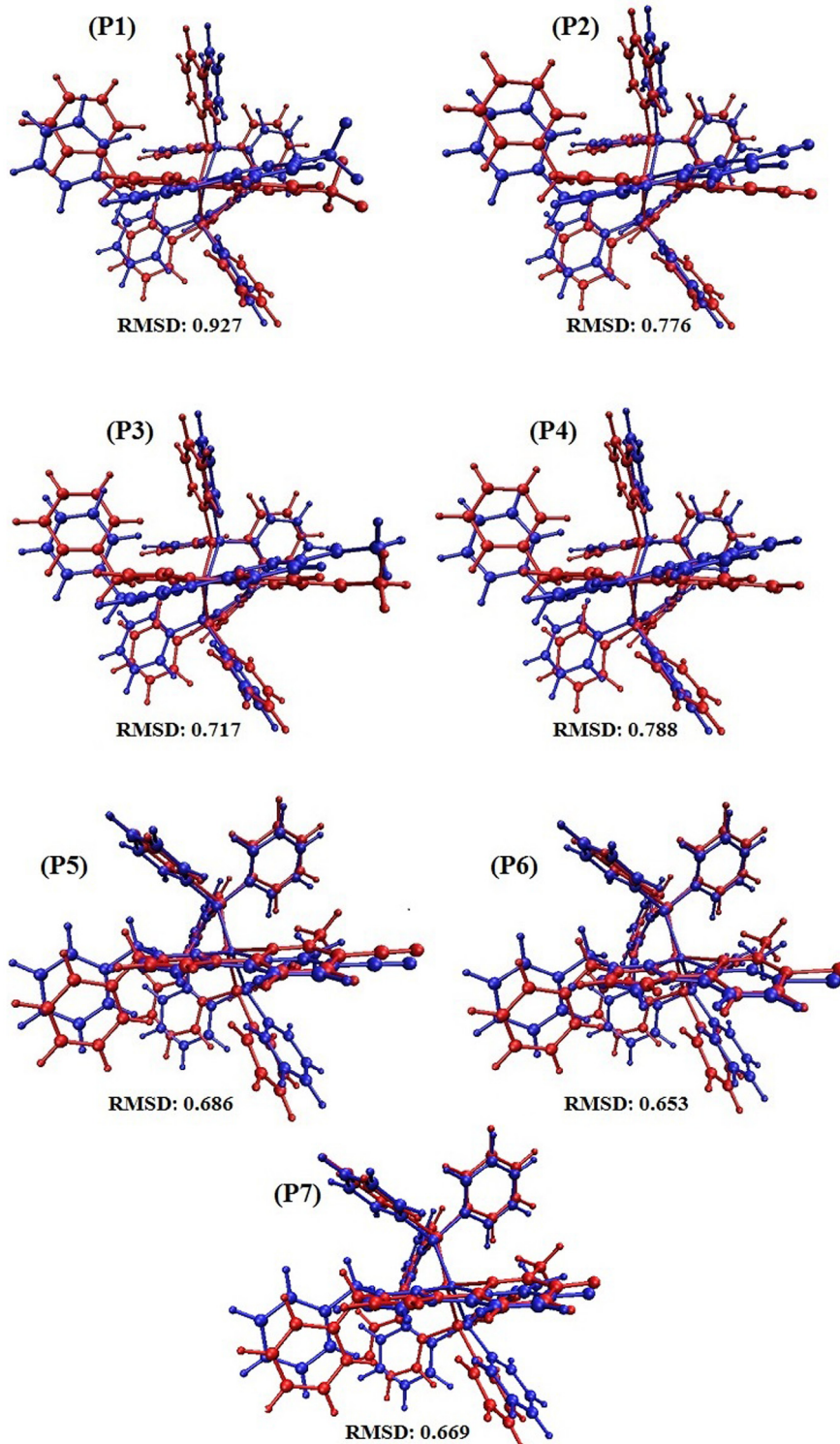


**Fig. 7.** Superimposition of the  $S_0$  (red) and  $T_1$  (blue) structures of studied complexes. (For interpretation of the references to colour in this figure legend, the reader is referred to the web version of this article.)

the other hand, the LUMO mainly distributes on the pyridine ring, and the LUMO energies exhibit large variation ( $-1.66$  eV to  $-2.56$  eV) for **P1-P7**. The addition of the substituents to the pyridine ring significantly affects LUMO than HOMO. The HOMO-LUMO gap gradually decreases following the order **P7** (4.33 eV) > **P6** (4.24 eV) > **P1** (3.96 eV) > **P5** (3.73 eV) > **P2** (3.63 eV) > **P3** (3.59 eV) > **P4** (3.46 eV). These data are concordant with the onset of the lowest-lying absorption bands in the experiment.

The low-energy transitions are calculated for **P1-P7** employing TDDFT method in  $\text{CH}_2\text{Cl}_2$  solution to further investigate the nat-

ure of the UV-Vis spectra. The corresponding transition characters are shown in **Table 2**. The simulated spectra of **P1-P7** are provided in [Fig. 2S in the Supporting Information](#), together with the experimental spectrum for the purpose of comparison. For all complexes, the red-shift of the calculated lowest-lying singlet-singlet excited state  $S_1$  can be observed in the following order: **P7** (335 nm) → **P6** (342 nm) → **P1** (372 nm) → **P5** (392 nm) → **P2** (406 nm) → **P3** (409 nm) → **P4** (428 nm), in line with the trend of HOMO-LUMO gaps mentioned above. The  $S_1$  state mainly originates from the HOMO → LUMO transition and

**Table 2**

Electronic absorptions of complexes **P1-P7** in  $\text{CH}_2\text{Cl}_2$  based on TDDFT calculations at the B3LYP/6-31g\*/LANL2DZ level, together with the experimental values.

	Excited state	Transition	Coeff	E(eV)/(nm)	Oscillator	Assign	Exptl/nm
<b>P1</b>	$S_1$	H → L	0.62900(79.1%)	3.32/372	0.0642	$\text{MLCT}_{(\text{Cu} \rightarrow \text{PyIm})}/\text{LLCT}_{(\text{POP} \rightarrow \text{PyIm})}$	355
	$S_7$	H → L + 4	0.69104(95.5%)	4.18/296	0.0782	$(\pi \rightarrow ^*\pi)_{(\text{POP})}/\text{MLCT}_{(\text{Cu} \rightarrow \text{POP})}$	272
	$S_{10}$	H → L + 5	0.69372(96.2%)	4.29/288	0.0673	$(\pi \rightarrow ^*\pi)_{(\text{POP})}/\text{MLCT}_{(\text{Cu} \rightarrow \text{POP})}$	272
	$S_{12}$	H → L + 5	0.66212(87.6%)	4.37/284	0.0467	$(\pi \rightarrow ^*\pi)_{(\text{POP})}/\text{MLCT}_{(\text{Cu} \rightarrow \text{POP})}$	272
	$S_{13}$	H-5 → L	0.43024(37.0%)	4.39/282	0.0543	$\text{LLCT}_{(\text{POP} \rightarrow \text{PyIm})}/\text{MLCT}_{(\text{Cu} \rightarrow \text{PyIm})}$	272
<b>P2</b>	$S_1$	H → L	0.68769(94.6%)	3.05/406	0.0581	$\text{LLCT}_{(\text{POP} \rightarrow \text{PyIm})}/\text{MLCT}_{(\text{Cu} \rightarrow \text{PyIm})}$	376
	$S_9$	H-5 → L	0.44404(39.4%)	4.15/298	0.0641	$\text{LLCT}_{(\text{POP} \rightarrow \text{PyIm})}/(\pi \rightarrow ^*\pi)_{(\text{PyIm})}$	276
		H-4 → L	0.35822(25.6%)			$\text{LLCT}_{(\text{Benzyl} \rightarrow \text{PyIm})}/(\pi \rightarrow ^*\pi)_{(\text{PyIm})}$	
		H-2 → L + 1	0.25078(12.6%)			$\text{MLCT}_{(\text{Cu} \rightarrow \text{POP})}/\text{LLCT}_{(\text{POP} \rightarrow \text{PyIm})}$	
	$S_{10}$	H → L + 3	0.68596(94.1%)	4.20/295	0.0831	$\text{MLCT}_{(\text{Cu} \rightarrow \text{POP})}/(\pi \rightarrow ^*\pi)_{(\text{POP})}$	276
<b>P3</b>	$S_1$	H-20 → L	0.28221(15.9%)	4.87/254	0.0994	$(\pi \rightarrow ^*\pi)_{(\text{PyIm})}/\text{MLCT}_{(\text{Cu} \rightarrow \text{PyIm})}$	248
		H-9 → L + 1	0.40275(32.4%)			$\text{LLCT}_{(\text{POP} \rightarrow \text{PyIm})}$	
	$S_9$	H → L	0.69531(96.7%)	3.03/409	0.0475	$\text{LLCT}_{(\text{POP} \rightarrow \text{PyIm})}/\text{MLCT}_{(\text{Cu} \rightarrow \text{COCH}_3)}$	369
		H-5 → L	-0.35591(25.3%)	4.12/300	0.1012	$\text{LLCT}_{(\text{Benzyl} \rightarrow \text{PyIm})}/\text{LLCT}_{(\text{POP} \rightarrow \text{COCH}_3)}$	282
		H-4 → L	0.54374(59.1%)			$\text{LLCT}_{(\text{Benzyl} \rightarrow \text{PyIm})}/(\pi \rightarrow ^*\pi)_{(\text{PyIm})}$	
<b>P4</b>	$S_1$	H → L + 3	0.68055(92.6%)	4.17/297	0.0672	$(\pi \rightarrow ^*\pi)_{(\text{POP})}/\text{MLCT}_{(\text{Cu} \rightarrow \text{POP})}$	282
	$S_9$	H → L + 4	0.67949(92.3%)	4.29/289	0.0752	$(\pi \rightarrow ^*\pi)_{(\text{POP})}/\text{MLCT}_{(\text{Cu} \rightarrow \text{POP})}$	282
		H → L + 5	0.67214(90.3%)	4.36/284	0.0673	$(\pi \rightarrow ^*\pi)_{(\text{POP})}/\text{MLCT}_{(\text{Cu} \rightarrow \text{POP})}$	282
	$S_{47}$	H-21 → L	-0.27774(15.4%)	4.89/253	0.1494	$\text{MLCT}_{(\text{Cu} \rightarrow \text{COCH}_3)}/\text{LLCT}_{(\text{PyIm} \rightarrow \text{COCH}_3)}$	251
		H-5 → L + 1	-0.23922(11.4%)			$\text{LLCT}_{(\text{Benzyl} \rightarrow \text{PyIm})}/\text{LLCT}_{(\text{POP} \rightarrow \text{PyIm})}/(\pi \rightarrow ^*\pi)_{(\text{PyIm})}$	
<b>P5</b>	$S_1$	H-4 → L + 1	0.31396(19.7%)			$(\pi \rightarrow ^*\pi)_{(\text{PyIm})}/\text{LLCT}_{(\text{Benzyl} \rightarrow \text{PyIm})}$	
		H → L + 1	0.22540(10.1%)			$\text{MLCT}_{(\text{Cu} \rightarrow \text{PyIm})}/\text{LLCT}_{(\text{POP} \rightarrow \text{PyIm})}$	
		H → L + 2	-0.26830(14.4%)			$\text{MLCT}_{(\text{Cu} \rightarrow \text{POP})}/(\pi \rightarrow ^*\pi)_{(\text{POP})}$	
	$S_8$	H → L	0.69524(96.6%)	2.89/428	0.0350	$\text{MLCT}_{(\text{Cu} \rightarrow \text{CHO})}/\text{LLCT}_{(\text{POP} \rightarrow \text{PyIm})}$	376
		H-5 → L	0.46033(42.3%)	4.01/308	0.0717	$\text{LLCT}_{(\text{POP} \rightarrow \text{PyIm})}/\text{LLCT}_{(\text{POP} \rightarrow \text{PyIm})}/(\pi \rightarrow ^*\pi)_{(\text{PyIm})}$	282
<b>P6</b>	$S_1$	H-4 → L	0.44165(39.0%)			$\text{LLCT}_{(\text{Benzyl} \rightarrow \text{PyIm})}$	
	$S_{14}$	H → L + 3	0.60043(72.1%)	4.19/295	0.0701	$(\pi \rightarrow ^*\pi)_{(\text{POP})}/\text{MLCT}_{(\text{Cu} \rightarrow \text{POP})}$	282
	$S_{19}$	H → L + 4	0.69380(96.2%)	4.29/288	0.0631	$(\pi \rightarrow ^*\pi)_{(\text{POP})}/\text{MLCT}_{(\text{Cu} \rightarrow \text{POP})}$	282
	$S_{34}$	H-2 → L + 2	0.57057(65.1%)	4.63/267	0.1153	$(\pi \rightarrow ^*\pi)_{(\text{POP})}/\text{MLCT}_{(\text{Cu} \rightarrow \text{POP})}$	253
		H → L + 7	0.29990(17.9%)			$(\pi \rightarrow ^*\pi)_{(\text{POP})}/\text{MLCT}_{(\text{Cu} \rightarrow \text{POP})}$	
<b>P7</b>	$S_1$	H-5 → L + 1	0.24839(12.3%)	4.79/258	0.1047	$\text{LLCT}_{(\text{POP} \rightarrow \text{PyIm})}/(\pi \rightarrow ^*\pi)_{(\text{PyIm})}/\text{LLCT}_{(\text{Benzyl} \rightarrow \text{PyIm})}$	253
		H-2 → L + 3	0.50466(50.9%)			$(\pi \rightarrow ^*\pi)_{(\text{POP})}/\text{MLCT}_{(\text{Cu} \rightarrow \text{POP})}$	
	$S_{43}$	H-21 → L	0.24171(11.6%)	4.80/258	0.1145	$\text{LLCT}_{(\text{POP} \rightarrow \text{PyIm})}/\text{LLCT}_{(\text{POP} \rightarrow \text{COH})}$	253
		H-2 → L + 3	0.30875(19.0%)			$(\pi \rightarrow ^*\pi)_{(\text{POP})}/\text{MLCT}_{(\text{Cu} \rightarrow \text{POP})}$	
		H-1 → L + 6	0.27314(14.9%)			$\text{MLCT}_{(\text{Cu} \rightarrow \text{POP})}$	
<b>P5</b>	$S_1$	H → L	0.69966(97.9%)	3.16/392	0.0673	$\text{LLCT}_{(\text{POP} \rightarrow \text{PyIm})}/\text{MLCT}_{(\text{Cu} \rightarrow \text{PyIm})}$	367
	$S_8$	H → L + 3	0.68495(93.8%)	4.15/298	0.0628	$(\pi \rightarrow ^*\pi)_{(\text{POP})}/\text{MLCT}_{(\text{Cu} \rightarrow \text{POP})}$	274
	$S_9$	H-5 → L	-0.32598(21.2%)	4.21/294	0.0980	$\text{LLCT}_{(\text{Benzyl} \rightarrow \text{PyIm})}/\text{LLCT}_{(\text{POP} \rightarrow \text{PyIm})}$	274
		H-4 → L	0.53207(56.6%)			$\text{LLCT}_{(\text{Benzyl} \rightarrow \text{PyIm})}/(\pi \rightarrow ^*\pi)_{(\text{PyIm})}$	
	$S_{10}$	H → L + 4	0.68606(94.1%)	4.31/287	0.0805	$(\pi \rightarrow ^*\pi)_{(\text{POP})}/\text{MLCT}_{(\text{Cu} \rightarrow \text{POP})}$	274
<b>P5</b>	$S_1$	H-1 → L + 2	0.63880(81.6%)	4.36/284	0.0694	$\text{MLCT}_{(\text{Cu} \rightarrow \text{POP})}/(\pi \rightarrow ^*\pi)_{(\text{POP})}/\text{LLCT}_{(\text{PyIm} \rightarrow \text{POP})}$	274
	$S_{11}$	H → L + 5	0.60753(73.8%)	4.41/280	0.0769	$(\pi \rightarrow ^*\pi)_{(\text{POP})}/\text{MLCT}_{(\text{Cu} \rightarrow \text{POP})}$	274
	$S_{14}$	H-18 → L	0.25011(12.5%)	4.93/251	0.1500	$\text{LLCT}_{(\text{POP} \rightarrow \text{PyIm})}/\text{MLCT}_{(\text{Cu} \rightarrow \text{PyIm})}$	248
		H-4 → L + 1	0.29233(17.1%)			$\text{LLCT}_{(\text{Benzyl} \rightarrow \text{PyIm})}/(\pi \rightarrow ^*\pi)_{(\text{PyIm})}$	
		H-3 → L + 3	0.26651(14.2%)			$(\pi \rightarrow ^*\pi)_{(\text{POP})}/\text{MLCT}_{(\text{Cu} \rightarrow \text{POP})}$	
<b>P6</b>	$S_1$	H → L	0.68756(94.5%)	3.62/342	0.0900	$\text{LLCT}_{(\text{POP} \rightarrow \text{PyIm})}/\text{MLCT}_{(\text{Cu} \rightarrow \text{PyIm})}$	334
	$S_8$	H → L + 4	0.68498(93.8%)	4.29/288	0.0749	$(\pi \rightarrow ^*\pi)_{(\text{POP})}/\text{MLCT}_{(\text{Cu} \rightarrow \text{POP})}$	282
	$S_{10}$	H → L + 5	0.67396(90.8%)	4.39/282	0.0620	$(\pi \rightarrow ^*\pi)_{(\text{POP})}/\text{MLCT}_{(\text{Cu} \rightarrow \text{POP})}$	282
	$S_{12}$	H-4 → L	0.46746(43.7%)	4.51/275	0.0724	$(\pi \rightarrow ^*\pi)_{(\text{POP})}$	282
		H-3 → L	0.36825(27.1%)			$\text{LLCT}_{(\text{POP} \rightarrow \text{PyIm})}$	
<b>P7</b>	$S_1$	H → L	0.65737(86.4%)	3.69/335	0.0786	$\text{LLCT}_{(\text{POP} \rightarrow \text{PyIm})}/\text{MLCT}_{(\text{Cu} \rightarrow \text{PyIm})}$	331
	$S_4$	H → L + 2	0.53040(56.2%)	4.11/302	0.0603	$\text{LLCT}_{(\text{POP} \rightarrow \text{PyIm})}/\text{MLCT}_{(\text{Cu} \rightarrow \text{PyIm})}$	272
		H → L + 3	0.43110(37.1%)			$(\pi \rightarrow ^*\pi)_{(\text{POP})}/\text{MLCT}_{(\text{Cu} \rightarrow \text{POP})}$	
	$S_8$	H → L + 4	0.65813(86.6%)	4.28/289	0.0465	$(\pi \rightarrow ^*\pi)_{(\text{POP})}/\text{MLCT}_{(\text{Cu} \rightarrow \text{POP})}$	272
	$S_{10}$	H → L + 5	0.67319(90.6%)	4.37/283	0.0688	$(\pi \rightarrow ^*\pi)_{(\text{POP})}/\text{MLCT}_{(\text{Cu} \rightarrow \text{POP})}$	272

can be regarded as  $^3\text{MLCT}/^3\text{LLCT}$  character for all complexes given that the HOMOs of **P1–P7** are located on the Cu (28.7%–32.7%) and POP (59.1%–62.7%), whereas their LUMOs dominantly reside on the PyIm ligand (63.2%–91.7%) (Fig. 3S, Table 2S–8S, Supporting Information). The complete assignments for the absorption transitions are collected in Table 2.

It is interesting to compare the ground geometry ( $S_0$ ) of **P2** with that of **P5** since their structures are similar, except for groups at the  $\alpha$ -position of the pyridine ring. Fig. 6 presents the optimized  $S_0$  structures of **P2** and **P5** in  $\text{CH}_2\text{Cl}_2$  solution. The larger difference observed is that the Cu–N1 bond length of **P5** (2.547 Å) is significantly longer compared with that of **P2** (2.353 Å), which is due to steric repulsion of the POP ligand with the methyl group at the  $\alpha$ -position of the pyridine ring. Thus, the interaction between the Cu (I) center and the pyridine moiety is weak and consequently decreases the probability of charge transfer from metal to the pyridine ring. This decrease is reflected by **P5** exhibiting a very low absorption ability observed experimentally in the MLCT region in contrast with **P2**.

It is well known that the structural flattening of the  $T_1$  states of the Cu(I) complexes significantly influence on the luminescence efficiency. Here, the spin-unrestricted U-DFT approach was employed to optimize the  $T_1$  state geometries of all the investigated complexes. A comparison between  $T_1$  and  $S_0$  geometries is provided in Fig. 7. For **P1–P4**, a marked flattening distortion in the  $T_1$  state was observed compared with the molecular structure in the  $S_0$  state. The pyridine ring in the  $T_1$  state was tilted out of the plane of the pyridine part in the  $S_0$  state. However, for **P5–P7**, one can see that the pyridine ring in the  $T_1$  state was almost super-

imposed with the pyridine ring in the  $S_0$  state, meaning that the degree of the flattening distortion is very small. In order to qualitatively evaluate the structural deviation from the  $S_0$  to the  $T_1$  states, the root-mean-square deviation (RMSD) between the  $S_0$  and the  $T_1$  states was calculated [42] and the calculated results are presented in Fig. 7. The RMSD values are in the range of 0.9–0.717 for **P1–P4**, which are significantly larger than those of **P5–P7** (0.653–0.686). These theoretical data reveal that the presence of the methyl substituent at the  $\alpha$ -position of the pyridine ring in **P5–P7** effectively suppresses the structural distortion of the excited states. Thus, the structural relaxation that occurred from the  $T_1$  to the  $S_0$  states is weakened, leading to the higher PLQY, which are consistent with the experimental values.

On the basis of the optimized  $T_1$  geometry, the TDDFT method was performed to calculate the triplet emission wavelengths of **P1–P7**. Here, the B3LYP functional underestimates the emission energy of the investigated Cu(I) complexes (Table 9S, Supporting Information). Thus, the emission energies were calculated at TD-CAM-B3LYP/6-31G(d)/LANL2DZ level. The results are presented in Table 3. The calculated emission wavelengths are red-shifted in the following order **P7** (501 nm)  $\rightarrow$  **P6** (508 nm)  $\rightarrow$  **P5** (531 nm)  $\rightarrow$  **P1** (573 nm)  $\rightarrow$  **P2** (578 nm), reproducing the experimental trend, except for **P3** and **P4**. The emitting states of all complexes originate mainly from the LUMO  $\rightarrow$  HOMO transitions. On the basis of the HOMO and LUMO compositions in the  $T_1$  state (Tables 10S, Supporting Information), the nature of the excited states can be assigned as the  $^3\text{MLCT}/^3\text{LLCT}$  characters for all complexes. The representative spin density plots of **P1**, **P2** and **P7** are shown in Fig. 8, further support the assignment of the emission state with the  $^3\text{MLCT}/^3\text{LLCT}$  character. The spin density distributions of other complexes are provided in Fig. 4S in the Supporting Information.

**Table 3**

Calculated emission wavelengths and  $T_1 \rightarrow S_0$  transition of **P1–P7** using TDDFT method with CAM-B3LYP functional. The experimental values are also provided.

	$\lambda_{\text{em}}^{\text{Calc}}/\text{nm}$	Configuration	Assignment	$\lambda_{\text{em}}^{\text{Exptl}}/\text{nm}$
<b>P1</b>	573	L $\rightarrow$ H (77.6%)	$^3\text{MLCT}/^3\text{LLCT}$	537
<b>P2</b>	578	L $\rightarrow$ H (75.2%)	$^3\text{MLCT}/^3\text{LLCT}$	547
<b>P3</b>	564	L $\rightarrow$ H (71.2%)	$^3\text{MLCT}/^3\text{LLCT}$	547
<b>P4</b>	574	L $\rightarrow$ H (70.6%)	$^3\text{MLCT}/^3\text{LLCT}$	547
<b>P5</b>	531	L $\rightarrow$ H (69.6%)	$^3\text{MLCT}/^3\text{LLCT}$	531
<b>P6</b>	508	L $\rightarrow$ H (71.3%)	$^3\text{MLCT}/^3\text{LLCT}$	515
<b>P7</b>	501	L $\rightarrow$ H (71.0%)	$^3\text{MLCT}/^3\text{LLCT}$	505

#### 4. Conclusion

In summary, seven Cu(I) complexes bearing the four-coordinate N-heterocyclic carbene ligands with different electron-withdrawing substituents are reported. **P1–P4** show the stronger MLCT absorption band compared with **P5–P6** with the methyl groups at the  $\alpha$ -position of the pyridine ring in the visible region. **P5–P7** with the emission maximum in the range of 505–531 nm show excel-

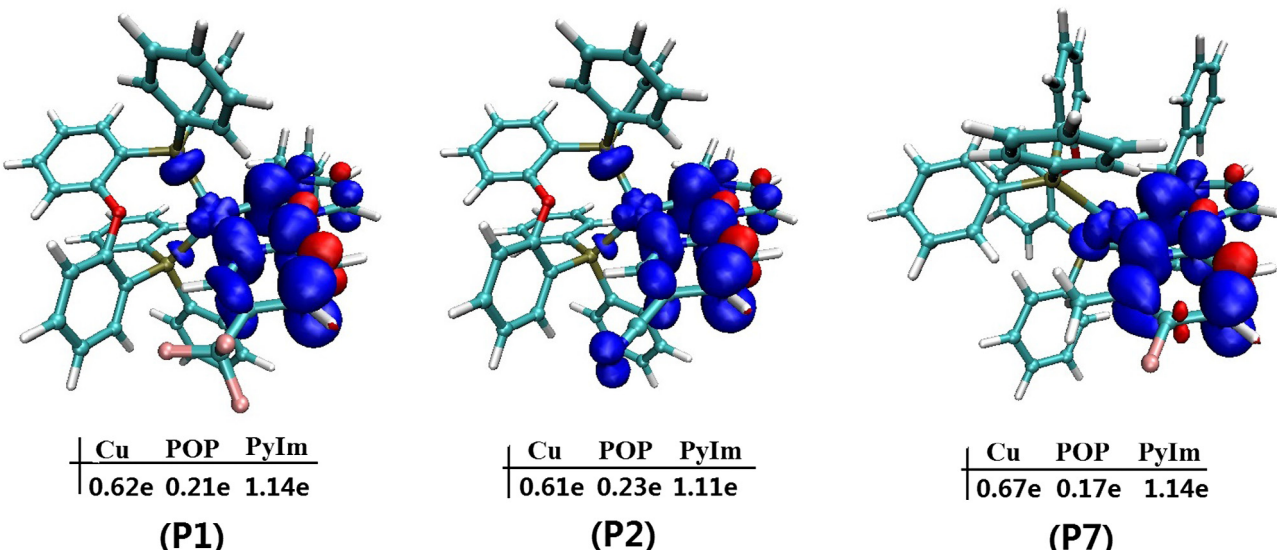


Fig. 8. Spin density distribution contours of **P1**, **P2** and **P7** (isovalue = 0.004) in the  $T_1$  state.

lent photophysical properties compared with **P1-P4**. The nature of the excited state can be assigned as the  $^3\text{MLCT}/^3\text{LLCT}$  character for all complexes. DFT and TDDFT calculations were performed to further explain these structure–property relationships.

### Declaration of Competing Interest

The authors declare that they have no known competing financial interests or personal relationships that could have appeared to influence the work reported in this paper.

### Acknowledgements

We thank the National Natural Science Foundation of China (No. 21563013 and 201961012) and the Natural Science Foundation of Jiangxi Province (No. 2010GZH0035) for their financial support. We are also grateful to the Guizhou University High Performance Computation Chemistry Laboratory (GHPCC) for their help with theoretical analysis.

### Appendix A. Supplementary data

Supplementary data to this article can be found online at <https://doi.org/10.1016/j.poly.2019.114240>.

### References

- [1] Y.G. Ma, W.H. Chan, X.M. Zhou, C.M. Che, Light-emitting diode device from a luminescent organocopper (I) compound, *New J. Chem.* 23 (1999) 263–265.
- [2] N. Mitsuhashi, G. Yasuyuki, E. Masanao, Electrophosphorescence from tetrameric copper (I)-amide cluster, *Chem. Lett.* 32 (2003) 32–33.
- [3] O. Moudam, A. Kaeser, B.D. Nicot, C. Duhayon, M. Höller, G. Accorsi, N. Armaroli, I. Séguy, J. Navarro, P. Destruel, J.F. Nierengarten, Electrophosphorescent homo-and heteroleptic copper (I) complexes prepared from various bis-phosphine ligands, *Chem. Commun.* 29 (2007) 3077–3079.
- [4] D.M. Zink, D. Volz, T. Baumann, M. Mydlak, H. Flügge, J. Friedrichs, M. Nieger, S. Bräse, Heteroleptic, dinuclear copper (I) complexes for application in organic light-emitting Diodes, *Chem. Mater.* 25 (2013) 4471–4486.
- [5] M. Osawa, M. Hoshino, M. Hashimoto, I. Kawata, S. Igawa, M. Yashima, Application of three-coordinate copper (I) complexes with halide ligands in organic light-emitting diodes that exhibit delayed fluorescence, *Dalton Trans.* 44 (2015) 8369–8378.
- [6] F.S. Wu, J. Li, H.B. Tong, Z.Y. Li, C. Adachi, A. Langlois, P.D. Harvey, L. Liu, W.Y. Wong, W.K. Wong, X.J. Zhu, Phosphorescent Cu (I) complexes based on bis (pyrazol-1-yl-methyl)-pyridine derivatives for organic light-emitting diodes, *J. Mater. Chem. C* 3 (2015) 138–146.
- [7] Q.S. Zhang, T. Komino, S.P. Huang, S. Matsunami, K. Goushi, C. Adachi, Triplet exciton confinement in green organic light-emitting diodes containing luminescent charge-transfer Cu (I) complexes, *Adv. Funct. Mater.* 22 (2012) 2327–2336.
- [8] G.F. Li, R.S. Nobuyasu, B.H. Zhang, Y. Geng, B. Yao, Z.Y. Xie, D.X. Zhu, G.G. Shan, W.L. Che, L.K. Yan, Z.M. Su, F.B. Dias, M.R. Bryce, Thermally activated delayed fluorescence in CuI complexes originating from restricted molecular vibrations, *Chem. - Eur. J.* 23 (2017) 11761–11766.
- [9] T. Hasegawa, A.I. Kobayashi, H. Ohara, M. Yoshida, M. Kato, Emission tuning of luminescent Copper (I) complexes by vapor-induced ligand exchange reactions, *Inorg. Chem.* 56 (2017) 4928–4936.
- [10] J.L. Wang, C.Y. Chai, S.X. Xua, F. Zhao, H.Y. Xia, Y.B. Wang, Synthesis, photophysical properties and DFT studies of the pyridine-imidazole (PyIm) Cu(I) complexes: impact of the pyridine ring functionalized by different substituents, *Inorg. Chim. Acta* 484 (2019) 237–244.
- [11] C. Yi, S.X. Xu, J.L. Wang, F. Zhao, H.Y. Xia, Y.B. Wang, Prolonging the emissive lifetimes of copper(I) complexes with  $^3\text{MLCT}$  and  $^3(\pi-\pi^*)$  state equilibria – a fluorene moiety as an “energy reservoir”, *Eur. J. Inorg. Chem.* 30 (2016) 4885–4890.
- [12] P. Aslanidis, V. Gaki, K. Chrissafis, M. Lalia-Kantouri, Luminescence and thermal behavior by simultaneous TG/DTG-DTA coupled with MS of neutral copper (I) complexes with heterocyclic thiones, *J. Therm. Anal. Calorim.* 103 (2010) 525–531.
- [13] S. Keller, A. Prescimone, H. Bolink, M. Sessolo, G. Longo, L. Martínez-Sarti, J.M. Junquera-Hernández, E.C. Constable, E. Ortí, C.E. Housecroft, Luminescent copper (I) complexes with bisphosphane and halogen-substituted 2, 2'-bipyridine ligands, *Dalton Trans.* 47 (2018) 14263–14276.
- [14] L.M. Zhang, B. Li, Z.M. Su, Realization of high-energy emission from  $[\text{Cu}(\text{N}-\text{N})(\text{P}-\text{P})]^+$  complexes for organic light-emitting diode applications, *J. Phys. Chem. C* 113 (2009) 13968–13973.
- [15] D.S. Zhang, Novel green-emitting copper(I) complexes with electron donors incorporated ligands: synthesis, photophysical properties, and electroluminescence performances, *J. Lumin.* 130 (2010) 1419–1424.
- [16] Z.J. Si, J. Li, B. Li, S.Y. Liu, W.L. Li, Bright electrophosphorescent devices based on sterically hindered spacer-containing Cu (I) complex, *J. Lumin.* 128 (2008) 1303–1306.
- [17] W.Y. Bai, L. Sun, A series of copper complexes with carbazole and oxadiazole moieties: synthesis, characterization and luminescence performance, *J. Lumin.* 132 (2012) 2697–2703.
- [18] V.A. Krylova, P.I. Djurovich, J.W. Aronson, R. Haiges, M.T. Whited, M.E. Thompson, Structural and photophysical studies of phosphorescent three-coordinate copper (I) complexes supported by an N-heterocyclic carbene ligand, *Organometallics* 31 (2012) 7983–7993.
- [19] R. Marion, F. Sguerra, F.D. Meo, E. Sauvageot, J.F. Lohier, R. Daniellou, J.L. Renaud, M. Linares, M. Hamel, S. Gaillard, NHC copper(I) complexes bearing dipyrimidamine ligands: synthesis, structural, and photoluminescent studies, *Inorg. Chem.* 53 (2014) (2014) 9181–9191.
- [20] V.A. Krylova, P.I. Djurovich, M.T. Whited, M.E. Thompson, Synthesis and characterization of phosphorescent three-coordinate Cu(I)-NHC complexes, *Chem. Commun.* 46 (2010) 6696–6698.
- [21] V.A. Krylova, P.I. Djurovich, B.L. Conley, R. Haiges, M.T. Whited, T.J. Williams, M.E. Thompson, Control of emission colour with N-heterocyclic carbene (NHC) ligands in phosphorescent three-coordinate Cu(I) complexes, *Chem. Commun.* 50 (2014) 7176–7179.
- [22] F. Dumur, Recent advances in organic light-emitting devices comprising copper complexes: a realistic approach for low-cost and highly emissive devices?, *Org. Electron.* 21 (2015) 27–39.
- [23] L.A. Schaper, S.J. Hock, W.A. Herrmann, F.E. Kühn, Synthesis and application of water-soluble NHC transition-metal complexes, *Angew. Chem. Int. Ed.* 52 (2012) 270–289.
- [24] S.B. Liu, S.X. Xua, J.L. Wang, F. Zhao, H.Y. Xia, Y.B. Wang, Four-coordinate N-heterocyclic carbene (NHC) copper (I) complexes with brightly luminescence properties, *J. Coord. Chem.* 70 (2017) 584–599.
- [25] J.L. Wang, S.B. Liu, S.X. Xu, F. Zhao, H.Y. Xia, Y.B. Wang, Four-coordinated copper(I) complexes containing variably substituted N-heterocyclic carbenes (NHCs): synthesis, photophysical properties and theoretical investigation, *J. Organomet. Chem.* 846 (2017) 351–359.
- [26] S.X. Xua, J.L. Wang, S.B. Liu, F. Zhao, H.Y. Xia, Y.B. Wang, Synthesis, photophysical properties, and computational studies of four-coordinate copper(I) complexes based on benzimidazolylidene N-heterocyclic carbene (NHC) ligands bearing aryl substituents, *J. Mol. Struct.* 1153 (2018) 12–19.
- [27] Z.Q. Wang, X.J. Suna, W.J. Fu, C. Xu, B.M. Ji, Four-coordinate Cu(I) complexes supported by N-heterocyclic carbene ligands bearing electron-donating/withdrawing groups: synthesis, structures and photophysical properties, *J. Lumin.* 204 (2018) 618–625.
- [28] Z.Q. Wang, C.J. Zheng, W.Z. Wang, C. Xu, B.M. Ji, X.H. Zhang, Synthesis, structure, and photophysical properties of two four-coordinate CuI-NHC complexes with efficient delayed fluorescence, *Inorg. Chem.* 55 (2016) 2157–2164.
- [29] E. Runge, E.K.U. Gross, Density-functional theory for time-dependent systems, *Phys. Rev. Lett.* 52 (1984) 997.
- [30] S.L. Mayo, B.D. Olafson, W.A. Goddard, DREIDING: a generic force field for molecular simulations, *J. Phys. Chem.* 94 (1990) 8897.
- [31] J.P. Perdew, K. Burke, M. Ernzerhof, Generalized gradient approximation made simple, *Phys. Rev. Lett.* 78 (1997) 1396.
- [32] M.J. Frisch, G.W. Trucks, H.B. Schlegel, G.E. Scuseria, M.A. Robb, J.R. Cheeseman, J.A. Montgomery Jr., T. Vreven, K.N. Kudin, J.C. Burant, J.M. Millam, S.S. Iyengar, J. Tomasi, V. Barone, M. Mennucci, M. Cossi, G. Scalmani, N. Rega, G.A. Petersson, H. Nakatsuji, M. Hada, M. Ehara, K. Toyota, R. Fukuda, J. Hasegawa, M. Ishida, T. Nakajima, Y. Honda, O. Kitao, H. Nakai, M. Klene, X. Li, J.E. Knox, H. P. Hratchian, J.B. Cross, C. Adamo, J. Jaramillo, R. Gomperts, R.E. Stratmann, O. Yazyev, A.J. Austin, R. Cammi, C. Pomelli, J.W. Ochterski, P.Y. Ayala, K. Morokuma, G.A. Voth, P. Salvador, J.J. Dannenberg, V.G. Zakrzewski, S. Dapprich, A.D. Daniels, M.C. Strain, O. Farkas, D.K. Malick, A.D. Rabuck, K. Raghavachari, J.B. Foresman, J.V. Ortiz, Q. Cui, A.G. Baboul, S. Clifford, J. Cioslowski, B.B. Stefanov, G. Liu, A. Liashenko, P. Piskorz, I. Komaromi, R.L. Martin, D.J. Fox, T. Keith, M.A. Allalam, C.Y. Peng, A. Nanayakkara, M. Challacombe, P.M.W. Gill, B. Johnson, W. Chen, M.W. Wong, C. Gonzalez, J.A. Pople, GAUSSIAN09, Revision A 02, Gaussian Inc., Pittsburgh, PA, 2009.
- [33] P.C. Hariharan, J.A. Pople, Accuracy of  $\text{AH}_n$  equilibrium geometries by single determinant molecular orbital theory, *Mol. Phys.* 27 (1974) 209.
- [34] M.S. Gordon, The isomers of silacyclopropane, *Chem. Phys. Lett.* 76 (1980) 163.
- [35] P.J. Hay, W.R. Wadt, Ab initio effective core potentials for molecular calculations. Potentials for K to Au including the outermost core orbitals, *J. Chem. Phys.* 82 (1985) 270.
- [36] M.E. Casida, C. Jamorski, K.C. Casida, D.R. Salahub, Molecular excitation energies to high-lying bound states from time-dependent density-functional response theory: characterization and correction of the time-dependent local density approximation ionization threshold, *J. Chem. Phys.* 108 (1998) 4439.
- [37] R.E. Stratmann, G.E. Scuseria, M.J. Frisch, An efficient implementation of time-dependent density-functional theory for the calculation of excitation energies of large molecules, *J. Chem. Phys.* 109 (1998) 8218.
- [38] T. Lu, F.W. Chen, Multiwfns: a multifunctional wavefunction analyzer, *J. Comput. Chem.* 33 (2012) 580.
- [39] W. Humphrey, A. Dalke, K. Schulten, VMD: visual molecular dynamics, *J. Mol. Graphics* 14 (1996) 33.

- [40] A.K. Verma, J. Singh, V.K. Sankar, R. Chaudhary, R. Chandra, Benzotriazole: an excellent ligand for Cu-catalyzed N-arylation of imidazoles with aryl and heteroaryl halides, *Tetrahedron Lett.* 48 (2007) 4207–4210.
- [41] G.J. Barbante, P.S. Francis, C.F. Hogan, P.R. Kheradmand, D.J.D. Wilson, P.J. Barnard, Electrochemiluminescent ruthenium(II) N-Heterocyclic carbene complexes: a combined experimental and theoretical study, *Inorg. Chem.* 52 (2013) 7448–7459.
- [42] E. Leoni, J. Mohanraj, M. Holler, M. Mohankumar, I. Nierengarten, F. Monti, A. Sourina-Saquet, B. Delavaux-Nicot, J.F. Nierengarten, N. Armarelli, Heteroleptic copper(I) complexes prepared from phenanthroline and bis-phosphine ligands: rationalization of the photophysical and electrochemical properties, *Inorg. Chem.* 57 (2018) 15537–15549.